Electronic Supplementary Material (ESI) for Chemical Communications.
This journal is © The Royal Society of Chemistry 2017

Electronic Supplementary Information For

Defects Engineering in Metal−Organic Frameworks: A new Strategy to Develop Applicable Actnide Sorbents

*Li-Yong Yuan,†[a] Ming Tian,†[ab] Jian-Hui Lan,[a] Xing-Zhong Cao,[a] Xiao-Lin Wang,[c] Zhi-Fang Chai,[a,d] John K. Gibson,[e] Wei-Qun Shi[a]**

[a] Laboratory of Nuclear Energy Chemistry, Institute of High Energy Physics, Chinese Academy of Sciences, Beijing 100049, China.

[b] School of Chemistry and Chemical Engineering, University of South China, Hengyang 421001, China.

[c] Institute of Nuclear Physics and Chemistry, China Academy of Engineering Physics, Mianyang, Sichuan 621900, China.

[d] School of Radiological&Interdisciplinary Sciences, Soochow University, Suzhou 215123, China.

[e] Chemical Sciences Division, Lawrence Berkeley National Laboratory (LBNL), Berkeley, California 94720, United States.

† These two authors contributed equally to this work.

*Corresponding author: E-mail: shiwq@ihep.ac.cn;

Corresponding information:

Prof. Dr. Wei-Qun Shi

Tel:86-10-88233968; E-mail: shiwq@ihep.ac.cn;

SI-1 Preparation of the MOFs with tunable defects

Synthesis of near defect-free UiO-66: $ZrCl_4$ (233 mg, 1.0 mmol), H_2BDC (332 mg, 2.0 mmol), and DMF (6 ml) were mixed in a Teflon liner at room temperature, then concentrated HCl (0.16 ml, 37%, 2.0 mmol) was added. The vessel was sealed, placed in an oven and heated to 220℃ and held for 20 h. After cooling to room temperature, the resulting white product was filtered off, washed with DMF to remove unreacted reagents, then washed again with acetone five times and dried under vacuum at 150 ^oC.

UiO-66 synthesis with modulator: $ZrCl_4$ (233 mg,1 mmol), terephthalic acid (H_2BDC, 166 mg, 1 mmol), and different equivalents of benzoic acid (HBC 5,10, 15, 20 mmol, respectively) with respect to H_2BDC were ultrasonically dissolved in 18 mL of DMF in a Pyrex vial. The synthesis mixture was transferred to a preheated oven at 120℃ for 48 h. After cooling down to room temperature, the products were isolated by centrifugation, washed with DMF and acetone five times, and dried at 80℃for 12 h. To extract the benzoic acid entrapped in the UiO-66, the as-synthesized samples were dispersed in 20 mL DMF with 0.4 mL concentrated HCl added at 90 ^oC for 12 h. The samples were then washed with DMF three times, and subsequently washed with acetone repeatedly to displace the trapped DMF. Finally, the obtained particles were dried at 150 ^oC in vacuo for 24 h. The samples were denoted as UiO-66-5D, UiO-66-10D, UiO-66-15D, and UiO-66-20D, respectively. (5, 10, 15, 20 are the molar equivalents of modulator with respect to H_2BDC in the initial synthesis mixture; D designates defects).

SI-2 Analytical techniques

The morphologies and microstructures of the samples were characterized with a field emission scanning electron microscopy (SEM, HITACHI S-4800). Powder X-ray diffraction (PXRD) patterns were obtained on a Bruker D8-Advance X-ray Diffractometer with a Cu Kα radiation. Thermogravimetric curves were recorded on a thermal gravimetric analyzer (TGA, TA Instruments, Q500) from 20-900 ^oC with a heating rate of 10 ^oC min^{-1} under an air flow. The N_2 sorption experiments were measured on a micromeritics ASAP 2020 HD88 instrument at liquid nitrogen temperature (-196 ^oC). The samples were degassed under vacuum at 120 ^oC before measurements. The specific surface area was calculated by the Brunauer–Emmett–Teller (BET) method. The pore size distributions were derived using the nonlocal density functional theory model. The total pore volume was evaluated by the single point method. Inductively coupled plasma optical emission spectrometer (ICP-OES, Horiba JY2000-2) was used to determine the residual concentration of U(VI) in supernatants in all the sorption experiments.

Table S1 The BET surface areas and pore volumes of UiO-66-DF and the defected UiO-66

Sample	Synthesis condition	BET surface area (m^2/g)	Total pore volume[a] (cm^3/g)
UiO-66-DF	220 °C, 20 h, no BC	790	0.42
UiO-66-5D	120 °C, 48 h, 5 eq BC	993	0.47
UiO-66-10D	120 °C, 48 h, 10 eq BC	1214	0.65
UiO-66-15D	120 °C, 48 h, 15 eq BC	1543	0.75
UiO-66-20D	120 °C, 48 h, 20 eq BC	1730	0.84

[a] Single point adsorption total pore volume of pores at $P/P_o = 0.975$

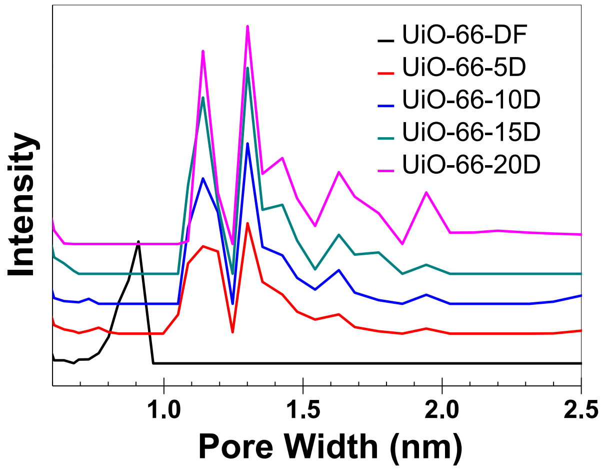

Fig. S1 pore size distributions of UiO-66-DF and the defected UiO-66s.

The positron annihilation lifetime spectroscopy (PALS) measurements were at room temperature using a standard fast-slow coincidence system with a time resolution of about 210 ps full width at half maximum (FWHM). The positron source (22Na, 16 μCi) was carrier free NaCl deposited between two 7 μm thick Kapton foils, and then sandwiched in two stacks of essentially identical pieces of sample (with a diameter of 1 cm and a thickness of 1.5 mm) ensuring that all positrons annihilate within the sample. All the positron lifetime spectra were recorded with total counts of $\sim 2 \times 10^6$. A standard nickel sample was used to calculate the fraction of positrons annihilating within the source and kapton foils. Correction for source components was performed in the analysis of positron lifetime spectra of the samples. The routine LT-9 was used for analysis of the positron lifetime spectra, taking into account the annihilation in the source; all of the collected spectra were analyzed by three exponential components.

Table S2 the fitting results obtained from PALS

Sample	τ_3(ns)	error(ns)	I_3(%)	error(ns)	*R* factor
UiO-66-20D	4.357	0.058	5.78	0.110	1.0649
UiO-66-DF	3.359	0.029	7.433	0.094	1.0967

TGA results for the prepared UiO-66s provided quantitative information about missing-linker defects. For perfect UiO-66, i.e. UiO-66-DF, an inner $Zr_6O_4(OH)_4$ core connects to 12 linkers, i.e. 1,4-benzene- dicarboxylate (BDC), while one linker bridges two metal cores, thus forming a structural unit of $Zr_6O_4(OH)_4(CO_2)_{12}$ or $Zr_6O_4(OH)_4(BDC)_6$. Accordingly, each unit in perfect UiO-66 includes 6 linkers. Upon heat treatment, the dehydroxylation of the $Zr_6O_4(OH)_4$ cluster starts at *ca.* 250 °C and ends at *ca.* 400 °C,[1] resulting in a Zr_6O_6 inner cluster ($Zr_6O_6(BDC)_6$). Complete collapse of the framework occurs at *ca.* 450 °C, forming the only solid product of ZrO_2. Since the molecular weight of $Zr_6O_6(BDC)_6$ is a factor of 2.2 higher than that of ZrO_2, the plateau in the temperature range of 400-450 °C for the solvent free material should ideally reach 220% when normalized to the final end weight as 100%. For the defected UiO-66s, however, the plateau is clearly below the expected value (highlighted by a horizontal dashed line in Fig. 1(d)), implying that the framework is less dense than that for nearly-undefected UiO-66. This is in accord with the absence of some linkers in the frameworks of defected UiO-66s.

SI-3 U(VI) sorption experiments

In a typical experiment, 4 mg of sorbent was added to either 10 mL of U(VI) solution in a flask (the solid-liquid ratio was 0.4 g/L). The control experiments were performed simultaneously using the identical U(VI) solution in the absence of the sorbent. After stirring for the desired time, the solid phase was separated from the aqueous solution using a 0.22 μm nylon membrane filter, and then the concentration of U(VI) in the aqueous phase was determined by ICP-OES (the detection limit is below 0.01 ppm). Before the ICP-OES measurement, the supernatant was diluted 25~100 times to ensure that the concentration of U(VI) in the analyzed solution was 1~5 μg/mL. The sorption capacity (*q*) of U(VI) were defined as $q=(C_0-C_e)\times V_{solution/msorbent}$, where C_0 and C_e represent the concentrations of metal ions in the aqueous phase for the control experiment and the sorption experiment after 2 h stirring, respectively; $m_{sorbent}$ and $V_{solution}$ designate the weight of the sorbent and the solution volume used in the sorption experiment, respectively. All values were measured in duplicate with the uncertainty within 5%.

SI-4. The sorption data fitted by isotherm models

The Langmuir model assumes that the sorption of metal ions occurs on a homogenous surface by monolayer sorption and there no interaction between adsorbed ions, with homogeneous binding sites and equivalent sorption energies. The linear equation of the Langmuir isotherm model is expressed as follows:

$$\frac{c_e}{q_e}=\frac{1}{q_m k_L}+\frac{c_e}{q_m} \qquad \text{(S1)}$$

where q_{m} is the maximum sorption capacity corresponding to complete monolayer coverage (mg/g) and k_{L} is a constant indirectly related to sorption capacity and energy of sorption (L/mg), which characterizes the affinity of the adsorbate and adsorbent. A linear plot was obtained when c_{e}/q_e was plotted against c_{e}; q_{m} and k_L were derived from the slope and intercept.

The Freundlich equation is an empirical equation based on sorption on a heterogeneous surface. The isotherm assumes that adsorbent surface sites have a spectrum of different binding energies. The linear equation can be expressed by:

$$\ln q_e=\ln k_F+\frac{1}{n}\ln c_e \qquad \text{(S2)}$$

where k_F and n are the Freundlich constants related to the sorption capacity and the sorption intensity, respectively. A linear relationship was obtained by plotting $\ln q_e$ against $\ln c_e$, and the values of k_F and n were calculated from the slope and intercept of the straight line.

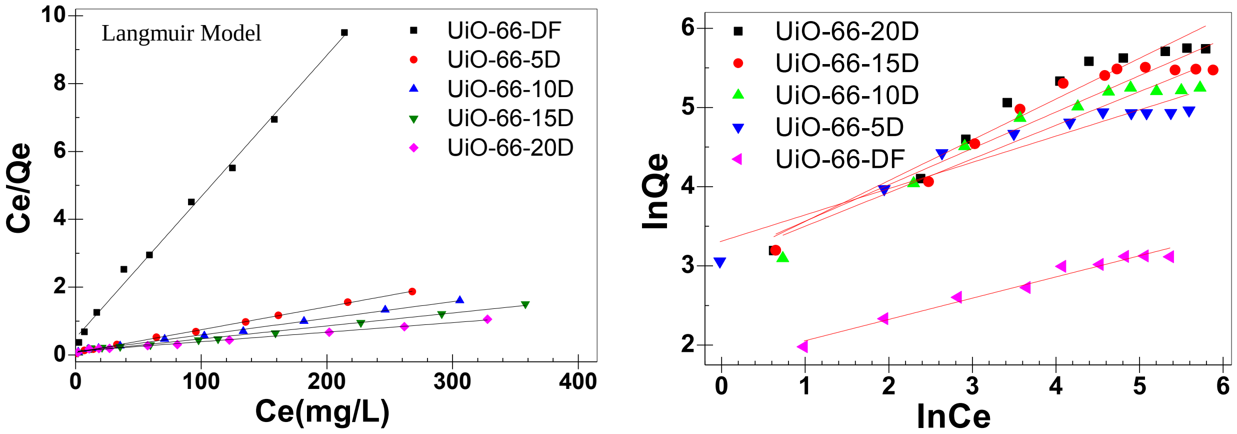

Fig. S2 Langmuir isotherm (left) and Freundlich isotherm (right) linearized plots for U(VI) sorption on UiO-66-DF and the defected UiO-66s

Table S3 comparison of parameters of Langmuir and Freundlich isotherms

	Langmuir			Freundlich		
	q_m(mg/g)	K_L(L/mg)	R^2	k_F(mg/g)	n	R^2
UiO-66-DF	24	0.0829	0.99	6	3.7318	0.97
UiO-66-5D	148	0.0981	0.999	27	3.0151	0.92
UiO-66-10D	203	0.0503	0.99	21	2.3523	0.91
UiO-66-15D	262	0.0419	0.99	23	2.2068	0.89
UiO-66-20D	357	0.0256	0.99	21	1.9418	0.94

SI-5 Elemental Analysis (via EDS) – Chlorine Content Studies

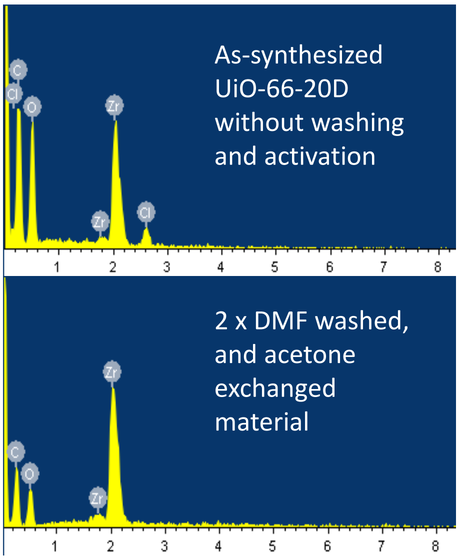

Fig. S3 EDS spectra of as-synthesized UiO-66-20D before (top) and after activation by DMF washing and acetone exchange (bottom)

Table S4 Quantitative data derived from the spectra presented in Fig. S3

Element	Atomic Ratio%	
	As-synthesized UiO-66-20D	DMF washed, and acetone exchanged material
C K	60.86	67.84
O K	36.72	27.67
Cl K	0.44	0
Zr L	1.98	4.49

Note: the light elements, such as carbon and oxygen cannot be reliably quantified due to the fact that the low energy X-rays that they emit do not efficiently penetrate the beryllium detector windows.

SI-6 Comparison of U(VI) uptake in UiO-66-20D and reported MOFs

Table S5 A summary of U(VI) uptake by MOFs

MOFs	Experimental pH	U(VI) uptake (mg g^{-1})	Ref.
UiO-66-NH_2	5.5 ±0.1	115	[2]
MIL-101-NH_2	5.5 ±0.1	90	[3]
MIL-101-ED	5.5 ±0.1	200	[3]
MIL-101-DETA	5.5 ±0.1	350	[3]
MOF-76(Y)	3.0 ±0.1	300	[4]
UiO-68-P(O)$(OEt)_2$	2.5	217	[5]
Zn-MOF-74	4.0	360	[6]
Zn(HBTC)(L) • $(H_2O)_2$	2.0	115	[7]
UiO-66-20D	5.0 ±0.1	350	This work

SI-7 Reusablity and selectivity test

Considering that little U(VI) sorption occurred in all the MOF sorbents at lower pH as denoted in Fig. 2a, regeneration of the MOF was performed by eluting the sorbed U(VI) using an acid solution, and the results were given in Table S6. It was found that a complete U(VI) leaching (> 99%) for UiO-66-20D can be easily achieved using a 0.2 mol/L HNO_3 solution, suggesting an apparent reversability of the U(VI) sorption into the defective UiO-66. Moreover, the comparison of PXRD patterns shows no discernable changes (Fig. 2d), implying that the MOF sorbents remain stable even after acidic desorption of U(VI).

Table S6. Regeneration and reusability of UiO-66-20D following U(VI) sorption

Desorption				[b]Reusability (mg/g)	
[a]HNO_3(mol/L)	0.2	0.1	0.05	Fresh	Reclaimed
Efficiency（%）	99.9	90.2	86.3	191	172

[a] Concentration of HNO_3 in the eluent;

[b] m/V=0.4 mg/mL, $[U]_{initial}$=100 mg/L, pH=5.0±0.05, t=4h.

To test selectivity of the present MOFs toward U(VI), the U(VI) sorption by UiO-66-DF and UiO-66-20D from an aqueous solution containing 0. 5 mmol/L Zn^{2+}, Cr^{3+}, Pb^{2+}, Ni^{2+}, Co^{2+}, Yb^{3+}, and Sr^{2+} was performed at pH 5.0, and the results were shown in Fig. S4. It was found that the defective UiO-66 exhibit superior U(VI) sorption over all the test competing metal ions, whereas for UiO-66-DF, the sorption of all the test metal ions including U(VI) kept in a low level. This result clearly indicates desirable selectivity of the defective UiO-66 towards U(VI).

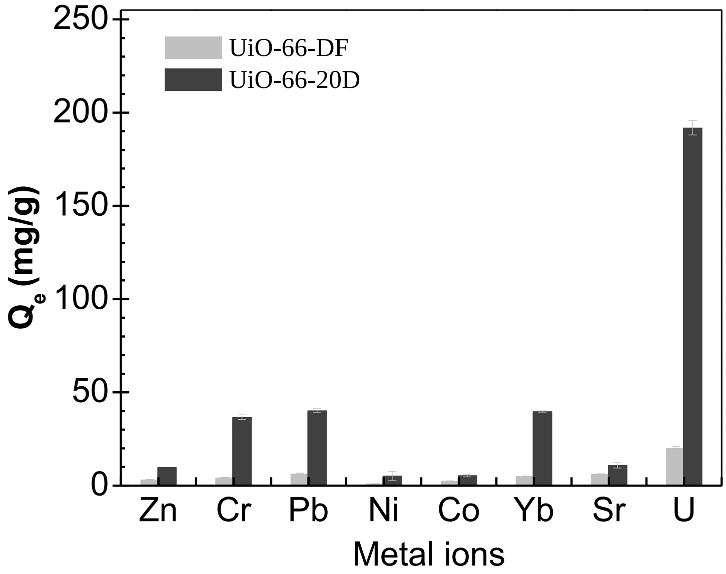

Fig. S4 competitive sorption of U(VI) by UiO-66-DF and UiO-66-20D from a solution containing competing metal ions. The concentration of all metal ions was 0.5 mmol/L. m/V=0.4 mg/mL, pH=5.0±0.05, t=4h.

SI-8 Molecular dynamics simulations

The migration of a uranyl ion in both perfect and defective frameworks of UiO-66 was modeled using classical molecular dynamic simulations implemented in the Lammps package. During all the simulations, the host material was modeled by a cubic 2×2×2 supercell with the lattice parameter of 41.493 Å. The measured pore volume is 0.47 cm^3/g[8], and correspondingly 1325 water molecules were inserted into the pores of the supercell to achieve water density at room temperature. Periodic boundary conditions were applied in all the three directions. The van der Waals interaction of framework atoms was described by the Lennard-Jones potential with the parameters taken from the Universal force field (UFF)[9]. The atomic charges for the perfect structure were derived from the work of Yang et al,[8] and those for the defective one were calculated at the PBE/6-31+g* level of theory (Fig. S3). The potential parameters developed by Pomogaev et al.[10] were used for the uranyl ion, along with the Simple Point Charge (SPC/E) water model[11] for the solvent water. The geometry of the water molecule was fixed using the SHAKE algorithm.[12] The geometric mixing rule was adopted to produce the interaction force field parameters between different species. The particle mesh-Ewald (PME) method was used for long range electrostatic interactions. The host material was kept rigid during simulations.

To estimate the migration path of uranyl in UiO-66, numerous free energy simulations were performed as displayed in Fig. 3 and Fig. S5,S6. For the perfect structure, we considered the following migration path: moving the uranyl ion through one window connecting an octahedral cage and one of its neighboring tetrahedral cages along the [111] direction (Fig. 3b, Fig. S5, S6). The above window consists of three linkers. Here, we have employed the umbrella sampling approach[13], in which the reaction coordinate to describe the migration event of uranyl was chosen. In this case, the distance of uranium relative to the center of the octahedral cage was chosen as the reaction coordinate. The interval of distance is set to be 0.3 Å, which was validated by plotting the histogram from individual trajectory of uranium along the reaction coordinate displayed in Figure S7. At all stages of the migration path, the system is in thermodynamic equilibrium. The distance of uranium relative to the center is harmonically restrained to 0.3 Å to allow the whole adsorption system to sample all possible configurations in the phase space. To do this, a spring force was applied to the uranium atom with the form,

$$V(\xi)=\frac{1}{2}k(\xi-\xi_0)^2 \qquad \text{(S3)}$$

where ξ_0 is the target reaction coordinate distance in Å and k is the force constant in kcal mol^{-1} Å^{-2}. The value of k is set to be 100 kcal mol^{-1} Å^{-2}. With the collected biased probability, we can then evaluated the unbiased probability of finding the system at ξ, $\rho(\xi)$, using the weighted histogram analysis method (WHAM)[14]. The free energy (or the potential of mean force, PMF), $W(\xi)$, is then given by the following equation.

$$W(\xi)=-RT\ln(\rho(\xi)) \qquad \text{(S4)}$$

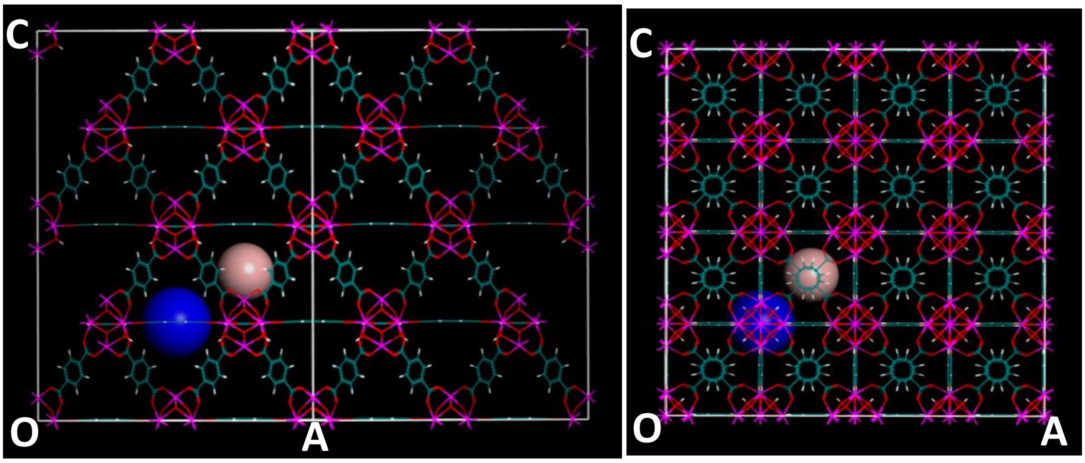

Fig. S5. Illustration of uranyl migration in perfect structure of UiO-66. Blue sphere and gray sphere denote the starting point and end point of the migration, respectively.

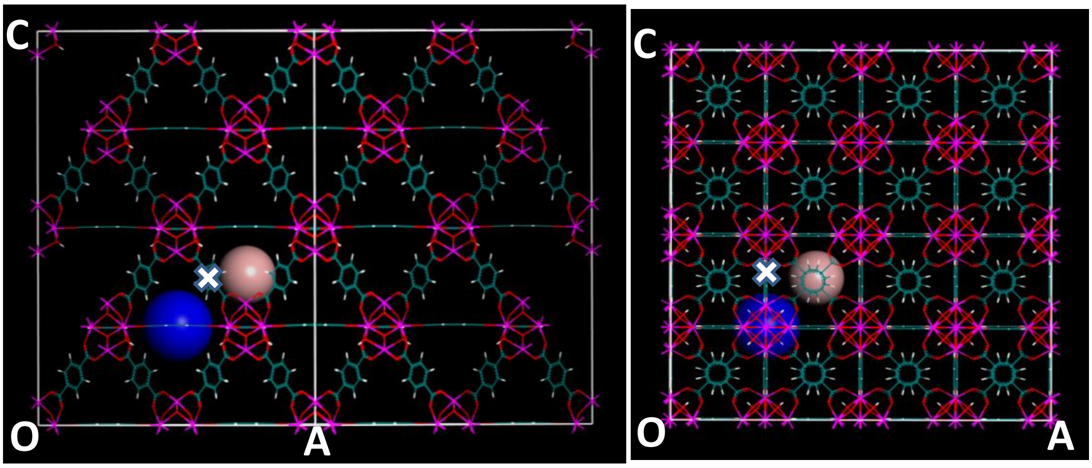

Fig. S6. Illustration of uranyl migration in defective UiO-66. Blue sphere and gray sphere denote the starting point and end point of the migration, respectively. The white X denotes where the aromatic linker is broken in the defective framework.

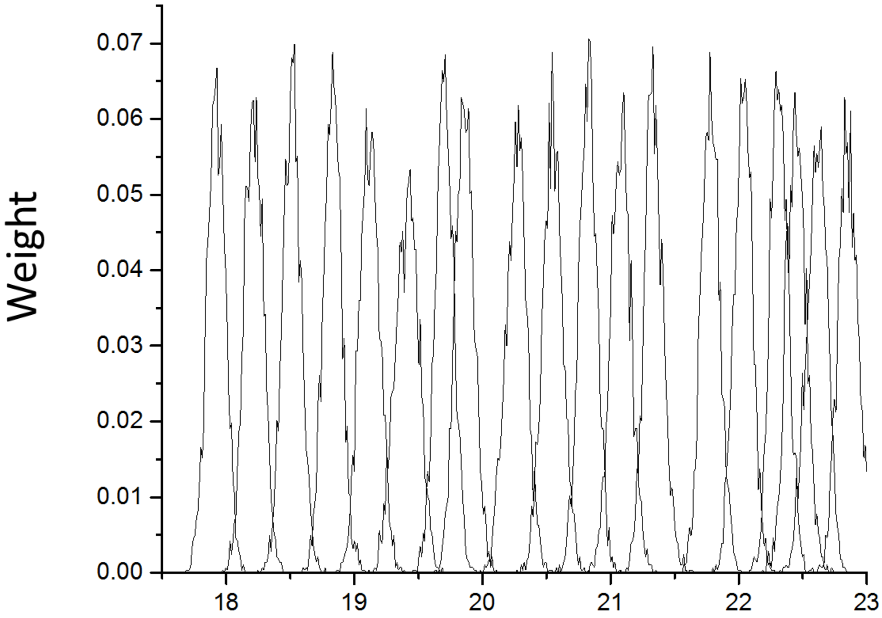

Fig. S7. Histograms from individual trajectory of uranium. The x-axis represents the distance of uranium relative to the origin of the simulation box along the [111] direction. And the starting point (0.25, 0.25, 0.25) corresponds to a distance of 18.17 A

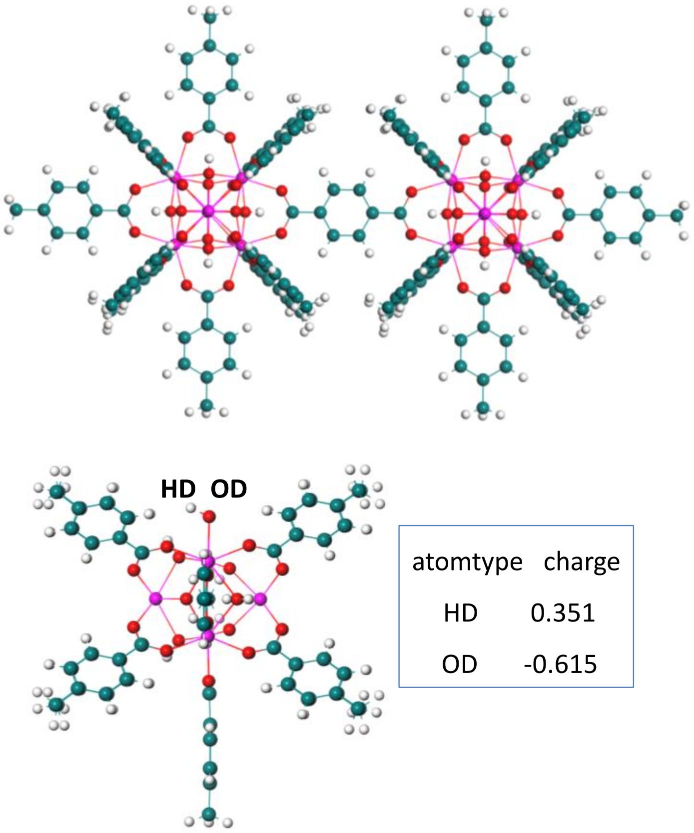

atomtype	charge
HD	0.351
OD	-0.615

Fig. S8 Models for atomic partial charge (e) calculation. HD and OD are the two new atom types we added to describe the newly formed hydroxyl groups bonded to Zr atoms in the defective UiO-66. Hydrogen, oxygen, carbon, Zr and U are colored in white, red, cyan, pink and blue, respectively.

In this section, we firstly probed the equilibration adsorption state of uranyl ion, $[UO_2(H_2O)_5]^{2+}$, by locating the ion at the center of the octahedral cage (as shown in yellow sphere in Fig. 3(a)). After an initial steepest descent energy minimization, 1 ns of canonical ensemble (NVT) simulations at 298.15 K were performed with a time step of 1 fs. Based on the predicted radial distribution function (RDF) (Fig. S9), we find that the uranyl ion at the equilibrium state is trapped around the center rather than migrating outside the cage. Within this cage, the uranyl ion is equatorially penta-coordinated to oxygen atoms of water in the first coordination sphere. The two sharp peaks at about 1.76 and 2.45 Å in Fig. S4 correspond to the predicted average U=O and U-O(H_2) bond lengths, which agree very well with experiments (1.76[15] and 2.42[16] Å, respectively).

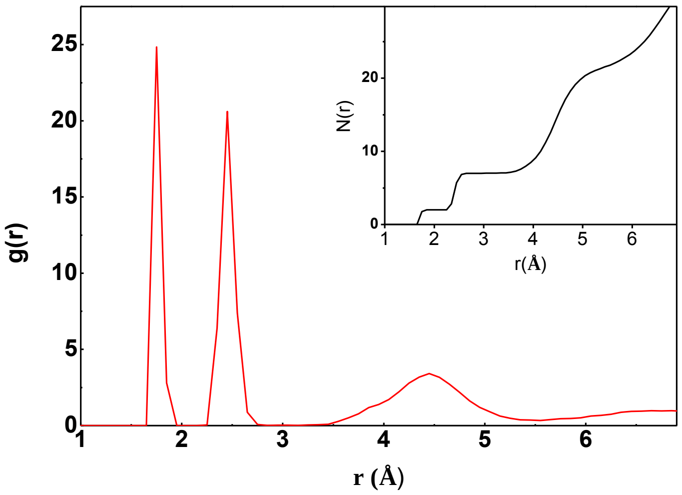

Fig. S9 The RDF and number integral (inset) of An=O and An-O(H$_2$) for UO$_2^{2+}$ in UiO-66, derived from the trajectory information of our MD simulation in NVT ensemble with the initial position of uranyl at the center of the octahedral cage.

REFERENCES

1. J. H. Cavka, S. Jakobsen, U. Olsbye, N. Guillou, C. Lamberti, S. Bordiga and K. P. Lillerud, *J. Am. Chem. Soc.*, 2008, **130**, 13850-13851.
2. B. C. Luo, L. Y. Yuan, Z. F. Chai, W. Q. Shi and Q. Tang, *J. Radioanal. Nucl. Chem.*, 2016, **307**, 269-276.
3. Z. Q. Bai, L. Y. Yuan, L. Zhu, Z. R. Liu, S. Q. Chu, L. R. Zheng, J. Zhang, Z. F. Chai and W. Q. Shi, *J. Mater. Chem. A*, 2015, **3**, 525-534.
4. W. T. Yang, Z. Q. Bai, W. Q. Shi, L. Y. Yuan, T. Tian, Z. F. Chai, H. Wang and Z. M. Sun, *Chem. Commun.*, 2013, **49**, 10415-10417.
5. M. Carboni, C. W. Abney, S. B. Liu and W. B. Lin, *Chem. Sci.*, 2013, **4**, 2396-2402.
6. L. Zhang, L. L. Wang, L. L. Gong, X. F. Feng, M. B. Luo and F. Luo, *J. Hazard. Mater.*, 2016, **311**, 30-36.
7. L. L. Wang, F. Luo, L. L. Dang, J. Q. Li, X. L. Wu, S. J. Liu and M. B. Luo, *J. Mater. Chem. A*, 2015, **3**, 13724-13730.
8. Q. Yang, V. Guillerm, F. Ragon, A. D. Wiersum, P. L. Llewellyn, C. Zhong, T. Devic, C. Serre and G. Maurin, *Chem. Commun.*, 2012, **48**, 9831-9833.
9. A. K. Rappe, C. J. Casewit, K. S. Colwell, W. A. G. Iii and W. M. Skiff, *J. Am. Chem. Soc.*, 1992, **114**, 10024-10035.
10. V. Pomogaev, S. P. Tiwari, N. Rai, G. S. Goff, W. Runde, W. F. Schneider and E. J. Maginn, *Phys.Chem. Chem. Phys.*, 2013, **15**, 15954-15963.
11. H. J. C. Berendsen, J. R. Grigera and T. P. Straatsma, *J. Phys. Chem.*, 1987, **91**, 6269-6271.
12. J. P. Ryckaert, G. Ciccotti and H. J. C. Berendsen, *J. Comput. Phys.*, 1977, **23**, 327-341.
13. S. Kumar, J. M. Rosenberg, D. Bouzida, R. H. Swendsen and P. A. Kollman, *J. Comput. Chem.*, 1992, **13**, 1011-1021.
14. B. Roux, *Comput. Phys. Commun.*, 1995, **91**, 275-282.
15. P. G. Allen, J. J. Bucher, D. K. Shuh, N. M. Edelstein and T. Reich, *Inorg. Chem.*, 1997, **36**, 4676-4683.
16. H. A. Thompson, G. E. Brown and G. A. Parks, *Am. Mineral.*, 1997, **82**, 483-496.